International Journal of Microwave and Wireless Technologies

cambridge.org/mrf

Gain-enhanced triple-band rectifier-integrated antenna for microwave wireless power transmission

Geriki Polaiah

Department of Physics, Bharat Institute of Technology, Hyderabad, Telangana, India

Research Paper

Cite this article: Polaiah G (2024) Gain-enhanced triple-band rectifier-integrated antenna for microwave wireless power transmission. *International Journal of Microwave and Wireless Technologies* **16**(3), 380–390. https://doi.org/10.1017/S1759078723000880

Received: 6 March 2023
Revised: 20 June 2023
Accepted: 4 July 2023

Keywords:
defected reflector structure; enhanced gain; fractal slot antenna; rectenna; voltage doubler rectifier; wireless power transfer

Email: polaiah@biet.ac.in

Abstract

This paper proposes a triple-band fractal slot antenna with enhanced gain operating at frequencies of 2.7, 3.5, and 4.8 GHz for microwave wireless power transmission. The antenna achieved more than 3 dB gain by preserving the symmetrical defected reflector structure behind it at a length of $0.54\lambda/4$, where λ is the wavelength in free space at 2.7 GHz. A 50 Ω micro-strip line coupled at 66 mm length helps feed the triple band slot antenna. The purpose of a triple-band rectifier circuit with an impedance network is to convert the radio frequency (RF) signal into direct current. The measurements reveal that the antenna's enhanced gain is 8.8 dB, and the rectifier's highest RF signal to direct current conversion efficiency is 74.3%. For the combined configuration unit of measure, the antenna is assimilated into the rectifier via back-to-back 50 Ω Sub Miniature Version A (SMA) connectors. The highest recorded efficiency of 49.67% was obtained for the rectenna at optimum values of 1 kΩ resistive load and −5 dBm power input. It has been revealed that the rectifier-integrated antenna presented is effective for low-input RF energy capture and power transmission.

Introduction

Nicola Tesla developed the idea of wireless power transmission in 1899 and experimentally validated it by conjugating two electromagnetic coils in the near-field. High-frequency radio wave sources were developed in 1930 by using high-power magnetron and klystron tubes. In 1960, W.C. Brown developed the first rectenna which can receive and rectify the high-frequency radio waves in far-field using the above high-frequency radio frequency (RF) sources [1]. The wireless power transmission is categorized into four types based on the distance and orientation of the transmitter and receiver. The wireless RF power is transferred in the near-field nonradiative mode by capacitive and inductive coupling, whereas in far-field radiative mode, the wireless power transfers via radio waves and diffused microwave beams. Nowadays, several antennas are being developed for the fabrication of various rectennas. Recent works include dual-frequency slot-loaded folded dipole antenna [2], broadband Yagi antenna array [3], dual-band microstrip antenna with enhanced gain [4], stacked dipole antenna [5], bow tie-shaped cross dipole antenna [6], dual-port triple-band antenna operating at Global System for Mobile Communications (GSM) and Universal Mobile Telecommunications System (UMTS) bands [7], dual-band printed monopole antenna [8], dual-band antennas of Composite right/left-handed (CRLH) metamaterial-based and tree-like structure for Wi-Fi and WiMAX frequencies [9, 10], aperture coupled right angle slot antenna [11], broadband slotted monopole antenna [12], dual-band loop antenna over Artificial Magnetic Conductor (AMC) surface [13], and triple band antenna for Long-Term Evolution (LTE) frequencies [14]. The rectifier circuit's input impedance and output voltage are mainly governed by the power input, equivalent resistance, and operating frequency. Nowadays, a large amount of RF power is radiated into space by cell towers, Wi-Fi routers, and digital TV towers, but this power is just available at a low level in the environment. High-gain antennas with high-efficiency rectifiers are essential for receiving low power input from ambient sources. Recently, various kinds of dual- and triple-band rectifiers [15–20], broadband rectifiers [21–25], reconfigurable rectifier topologies [26, 27], rectifiers with extended operating bandwidth and load resistance [28–30], resistance compression network-based rectifiers [31, 32], rectifiers with Field-effect transistor (FET) mounted to diode [33], single- and multi-stage voltage doubler rectifiers [34–37], and rectifier arrays and impedance matching network systems [38–42] have been extensively developed to improve the efficiency. The optimization of load impedance and power input is absolutely essential for the implementation of any rectifier because the rectifier has highest efficiency only at a particular load resistance and input power. The procedure for streamlining resistive load and power input is mentioned in a few of the above rectifiers.

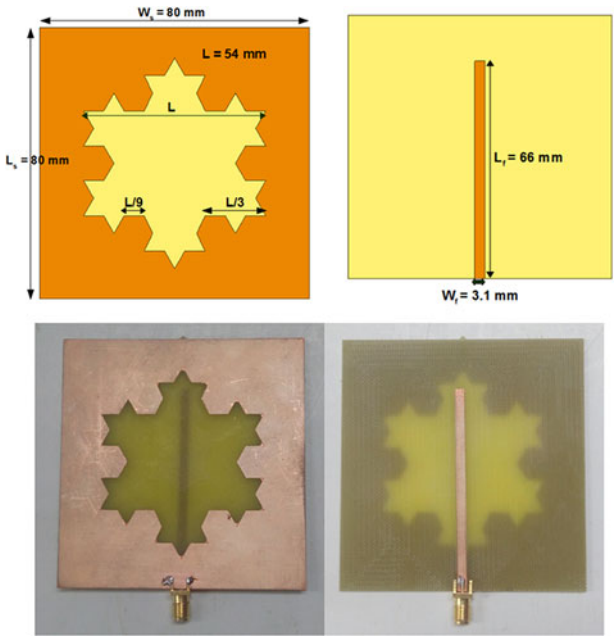

Figure 1. The proposed triple-band fractal slot antenna without reflector has a layout and construction prototypes.

The change in output voltage and calculated efficiency of the rectifier at various fixed input powers and the variation of output voltage and estimated rectifier efficiency for different input powers and at fixed load resistance could also be described in the literature. This perfectly evaluates the rectifier's behavior and officially ends the high conversion efficiency values of load resistance and power input at fixed resonant frequencies prior to the fabrication of the proposed prototype. The conference paper [43] would, however, report on a triple-band antenna with enhanced gain that used a complete metal layer reflective surface for RF energy harvesting. This work describes gain improvement by putting the reflective surface at a distance of $\lambda/4$ because the present work has been using a defected reflector structure (DRS) for antenna gain enhancement. As a direct consequence, the distance between both the antenna as well as the reflector tends to decrease and is less than $\lambda/4$. Apart from that, developing both the antenna and the rectifier at exactly equal multiband resonance frequency is a challenge. A symmetrical slot antenna coupled with an optimum feed length (FL) is proposed in this work for microwave energy capture and power transmission. The presented symmetrical slot is compactly structured to geometrical dimensions precalculated ahead of time. This antenna is interconnected to a rectifier to develop a rectifier-integrated antenna. A rectifier that uses only one Villard voltage multiplier with impedance network is also developed to rectify the obtained radio wave power into DC, with just conversion efficiency of more than 70%. The proposed antenna and reflector are designed, fabricated, and measured for required experimental results. The experimental results agree exceptionally well with the numerical simulations. Section "Receiving antenna" focuses on the presented triple-band antenna design features and analysis of the findings. Section "Rectifier circuit" explains the triple-band rectifier methodological approach and discussion of results. Section "Rectenna measurement" also indicates the measurement process and actual outcomes of the interconnected arrangement of the rectifier-integrated antenna. Finally, in section "Conclusion," the researcher debated on the paper's conclusion.

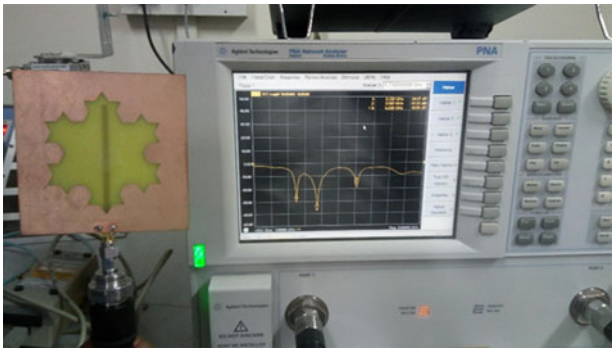

Figure 2. Measurement of the proposed antenna's coefficient of reflection ($|S_{11}|$) frequency dependence.

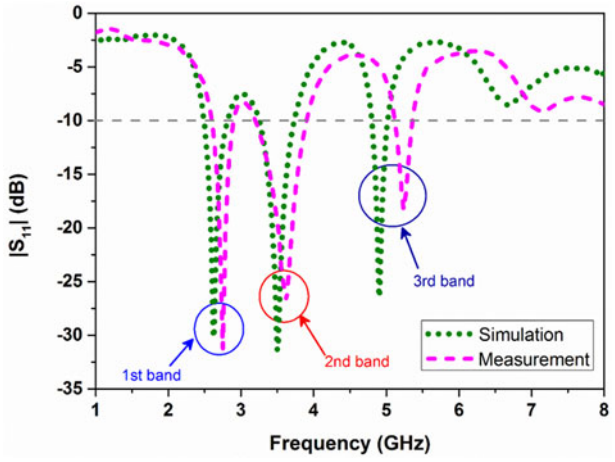

Figure 3. The magnitude of the coefficient of reflection ($|S_{11}|$) frequency dependence of the antenna without the need for a reflector was simulated and measured.

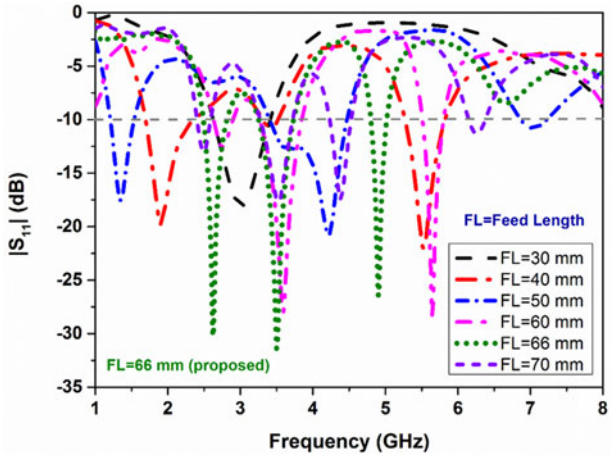

Figure 4. Parametric analysis of variation of feed length (FL) without reflector.

Receiving antenna

Antenna design and analysis

To get a fairly low RF energy from specific frequencies, a multiband antenna with increased gain is strongly recommended. On the top of the ground plane, an equiangular slot is structured. The feed line

https://doi.org/10.1017/S1759078723000880 Published online by Cambridge University Press

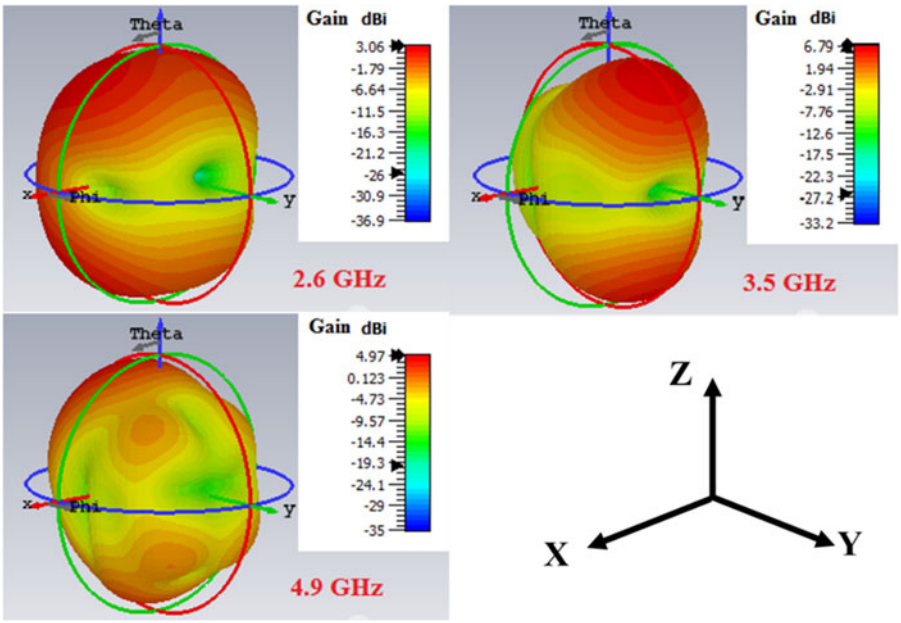

Figure 5. The computational results of the proposed antenna's three-dimensional radiation patterns without a reflector.

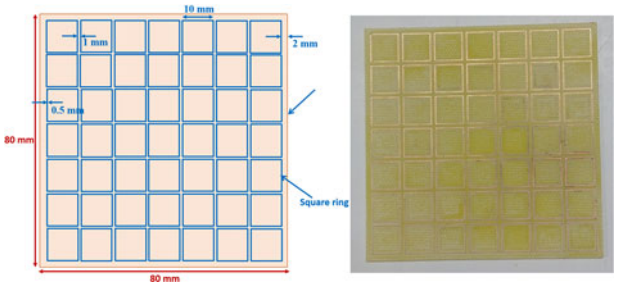

Figure 6. Schematic and fabrication prototypes of the proposed planar defected reflector structure (DRS).

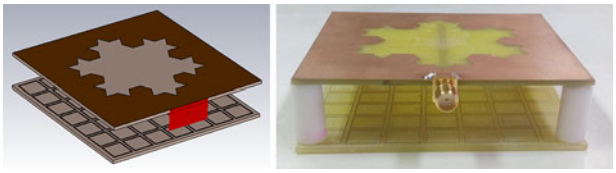

Figure 7. Computational and experimental configurations of the antenna with DRS reflector.

is intended to run behind the dielectric substrate. The dielectric substrate attempts to measure 80×80 mm^2. The equiangular slotted antenna is designed on an FR4 dielectric substrate with a thickness of 1.6 mm.

The geometrical equilateral triangular slot has a side length (L) of 54 mm. A 50 Ω resistive microstrip transmission line with an optimum distance (L_f) of 66 mm and a width (W_f) of 3.1 mm energises this suggested slot. According to [44], the idea of variable FL has been considered. By keeping the slot dimension unchanged, the length of the feed line is only varied. Figure 1 illustrates the layout and construction designs of the spatial design slot antenna without reflector. The requisite computer models for the presented antenna's assessment were decided to be carried out with the comprehensive electromagnetic simulation platform CST Studio Suite.

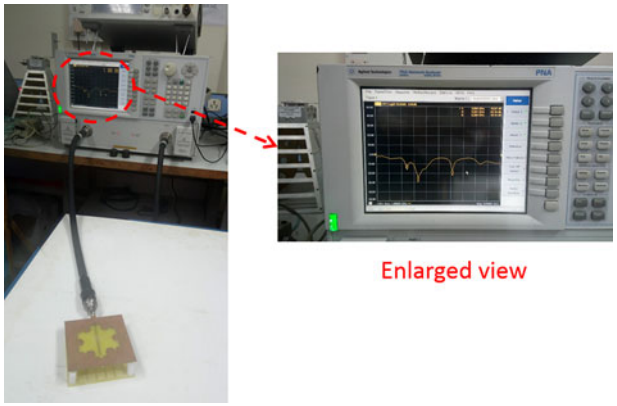

Figure 8. The magnitude of the coefficient of reflection ($|S_{11}|$) frequency dependence of the proposed antenna with DRS reflective surface was measured.

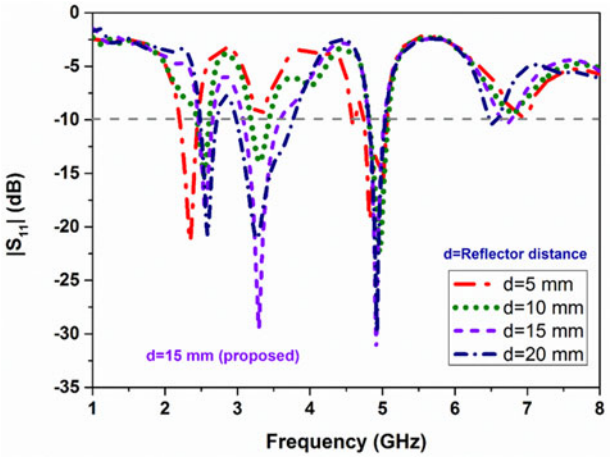

Figure 9. The parameterized evaluation of the antenna's simulated data with distance (d).

Before designing the proposed slot on a simulation tool, the important dimensional sizes are determined by calculation.

https://doi.org/10.1017/S1759078723000880 Published online by Cambridge University Press

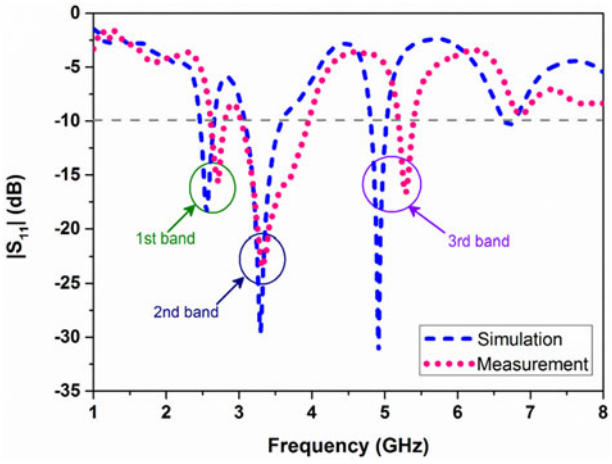

Figure 10. The magnitude of the coefficient of reflection ($|S_{11}|$) with DRS reflective surface was designed to simulate and analyzed.

Simulation and measurement results

After the successful completion of all requisite simulation studies, this same proposed antenna is crafted on the S103 LPKF ProtoMat machine. For linking to the RF cable, the antenna is connected to a 50 Ω inbuilt impedance SubMiniature Version A (SMA) connector. The E8363C Power Network Analyzer (PNA) network analyzer is used for measuring the antenna's input reflection coefficient initially. Figure 2 demonstrates the variation of $|S_{11}|$ versus resonant frequency of the designed antenna without the need for a reflective surface.

Simulation and measurement results are plotted in a single graph for comparison. Figure 3 represents the computation and recorded outcomes of the proposed antenna's reflection coefficient ($|S_{11}|$) versus frequency. In accordance with the numerical simulations, the antenna resonates at 2.6, 3.5, and 4.9 GHz. The measuring device results were in close agreement with the numerical simulations. The characteristic impedance of the measured result ($|S_{11}|$) is less than −15 dB for all three bands. Figure 4 shows the parameterized investigation of the proposed antenna's FL versus switching frequency. The achievement of $|S_{11}|$ is analyzed by expanding the FL by 10 mm every time from 30 to 70 mm. At an FL of 66 mm, it is feasible to obtain consistent triple bands of WLAN and WiMAX frequencies. The simulation findings reveal that for the three control RFs, the characteristic impedance was lower than −25 dB. Figure 5 illustrates the computation outcomes of the proposed antenna's three-dimensional beams without the need for a reflective surface. The radiation patterns show that at the resonant frequencies of 2.6, 3.5, and 4.9 GHz the realized gain of more than 3 dB has been achieved. The above patterns are bi-directional and directed along the $+Z$ and $-Z$ axes. The gain of the antenna has been enhanced while attempting to maintain it above the operating frequencies by employing a periodic array of a planar structure. The following section briefly describes the architectural features, construction, and measurement of a symmetrical DRS planar array, along with the proposed antenna.

Defected reflector structure

Figure 6 depicts the suggested planar DRS layout and construction models. This reflector structure is modeled after the reflector introduced in [4], with the objective of increasing the antenna's gain at three operating frequencies without attempting to change their resonances. The size of the reflective surface is 80 × 80 mm^2, which really is equivalent to the size of the antenna. Square rings of a 7 × 7 array are spaced 1 mm apart within this reflector. The square ring's side length is 10 mm and its thickness is 0.5 mm. The distance between the last square ring and the substrate end is 2 mm. These square rings are designed periodically on the substrate, with no metal printed on the bottom side. The presented reflector is constructed on a substrate surface (FR4) with properties similar to those used in antenna design.

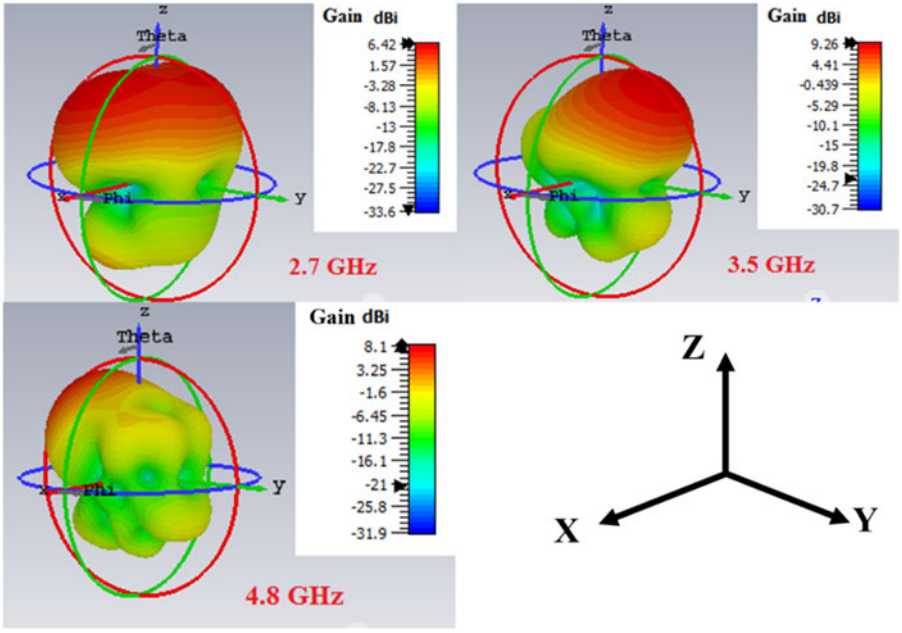

Figure 11. Radiation patterns with DRS reflector at three operating frequencies were simulated.

https://doi.org/10.1017/S1759078723000880 Published online by Cambridge University Press

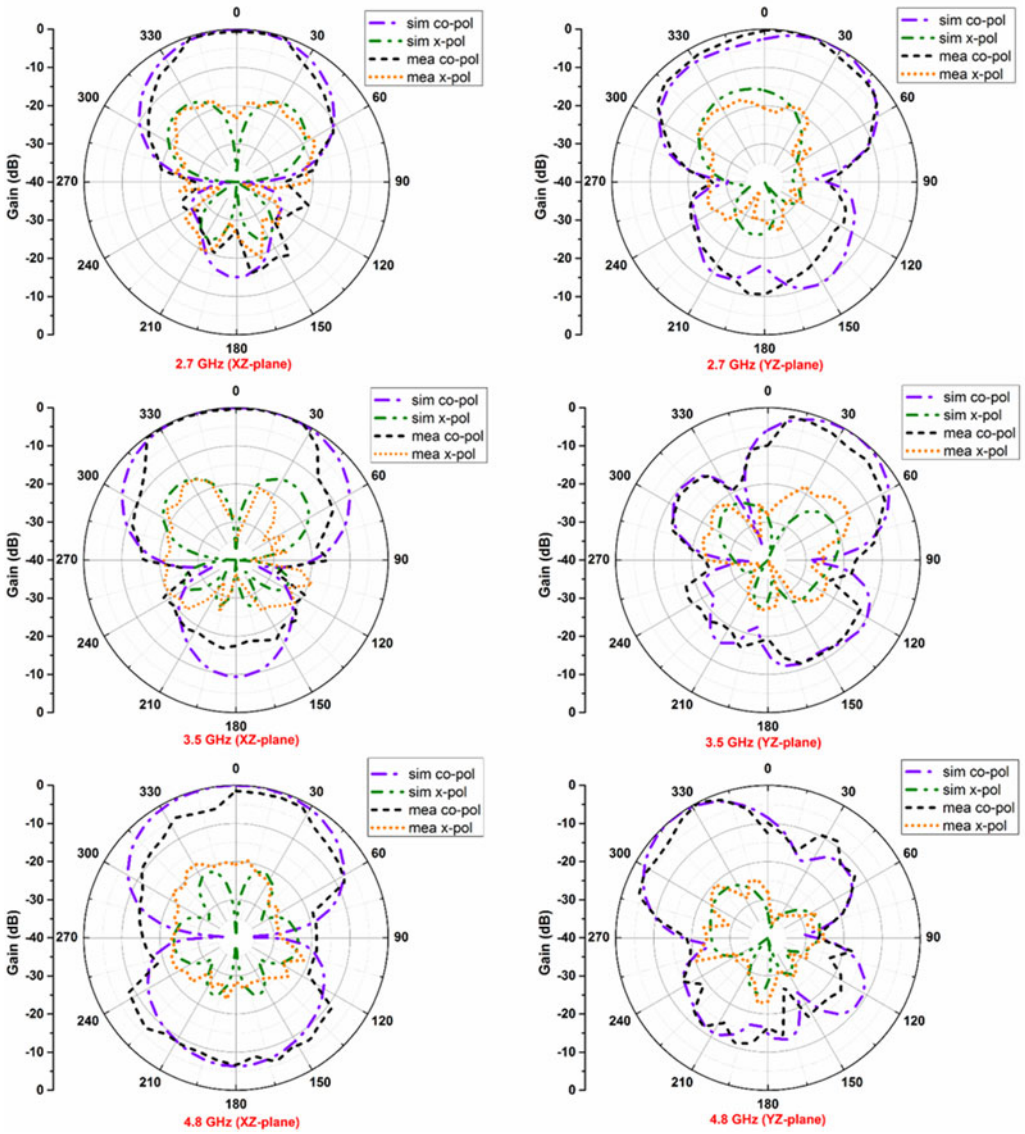

Figure 12. Normalized radiation patterns with DRS reflector.

Results of the antenna with DRS

Figure 7 characterizes computation and construction configuration settings of the antenna with DRS. Teflon sticks with a diameter of 8 mm are employed to facilitate the antenna, which would be kept separate from the reflector. The distance between the antenna and the reflector is streamlined to be $0.54\lambda/4$ (approximately 15 mm). Figure 8 illustrates a picture of the coefficient of reflection ($|S_{11}|$) function of frequency of the antenna with DRS. The network analyzer's display is also enlarged for viewing the triple resonant bands. Figure 9 shows that the antenna's simulation results with reflector distance (d). The simulation model for the antenna with the reflective surface is again managed to be performed by vastly differing the reflector distance of 5 mm each time from $d = 5$ mm to $d = 20$ mm. At a reflector length of $d = 15$ mm, the directional antennas' continuous resonance frequency tunes of 2.7, 3.5, and 4.8 GHz related frequency bands are acquired. Figure 10 conveys the modeling and evaluated findings for the proposed directional antennas' coefficient of reflection ($|S_{11}|$) frequency dependence. The first two bands are well suited, whereas the third frequency range has a small gap with the simulated results due to impedance mismatch in tolerance levels.

The defected reflector structure (DRS) is suitable to place behind the antenna at a small distance to improve the gain of the proposed antenna. Figure 11 portrays the modeling outcomes of the proposed antenna's three-dimensional radiation patterns with DRS at three frequency bands. Gain values of more than 3 dB were achieved without attempting to change the resonance frequency. DRS achieved the enhanced gains of 6.42, 9.26, and 8.1 dB at frequencies of 2.7, 3.5, and 4.8 GHz, respectively. The main beam of unidirectional radiation patterns for the three frequencies could really be observed to be directly aimed toward the $+Z$-direction. A transmit antenna with a broadband gain is employed for gain and radiation pattern measurement techniques. The antenna is positioned at the receiving end, at a distance of 1.4 m from the transmit antenna (horn). To measure the antenna

https://doi.org/10.1017/S1759078723000880 Published online by Cambridge University Press

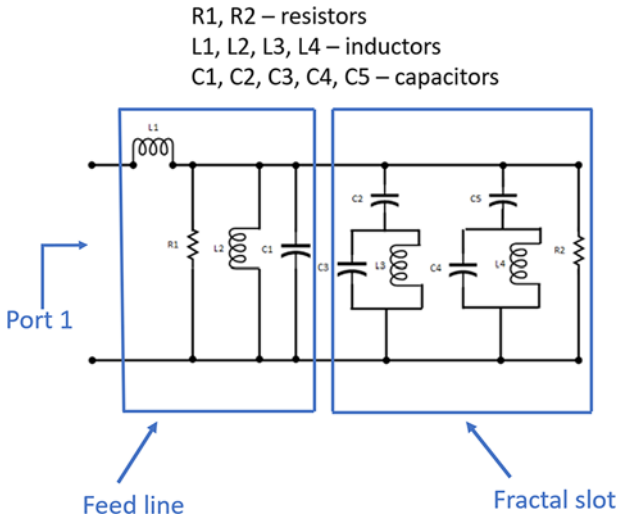

Figure 13. The proposed antenna equivalent circuit.

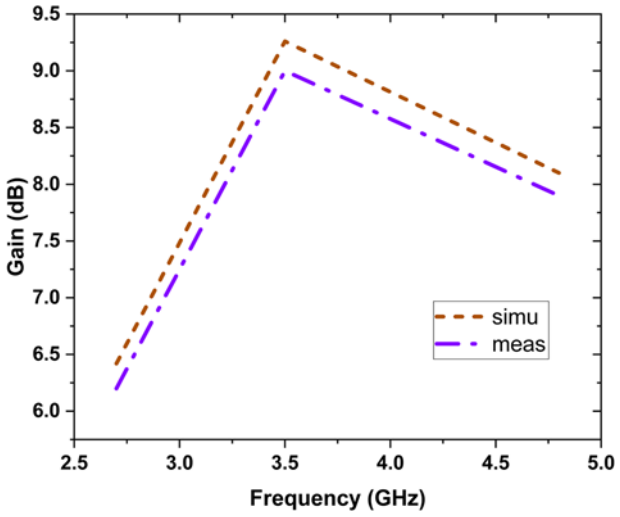

Figure 14. The gain of the proposed antenna (simulation and measurement results).

gain and radiation patterns, network analyzer port-1 is attached to the transmit antenna and port-2 is linked to the receiver side (proposed). The radiation patterns at every one of the three operating frequencies are measured and displayed along with the the numerical simulations. With DRS, the proposed antenna measured gain values of 6.1, 8.8, and 7.6 dB at harmonic resonance of 2.7, 3.5, and 4.8 GHz, respectively. The field radiation patterns are standardized to zero, which would be comparable toward how numerical simulations are linearly proportional in the CST simulation software. The modeling and measurement data of relatively stable patterns of the suggested antenna with DRS at mainly two planes of XZ-plane ($\phi = 0^{\circ}$) and YZ-plane ($\phi = 90^{\circ}$) patterns are displayed in Fig. 12. It should be acknowledged that the this double patterns are uni-directive and focused along the $+Z$-axis. To enhance gain and radiation effectiveness, a metallic reflector is usually situated at a distance of $\lambda/4$ behind the antenna. The DRS is positioned behind the antenna at a length of $0.54\lambda/4$ in the prototype architecture. The designed antenna has the benefits of a compact design, simple fabrication, and connection adaptability to the rectifier.

The proposed antenna's equivalent circuit is shown in Fig. 13. The parallel RLC circuit and inductor in series constitute the microstrip feed line. The fractal slot and its coupling with the microstrip feed line are represented by the two parallel LC circuits that are both in series with capacitors. Simulation and measured results of gain of the proposed antenna is shown in Fig. 14. Experimental results are well in agreement with the simulation results.

Rectifier circuit

Rectifier design and analysis

For converting collected high-frequency microwave power into DC, a microstrip transmission line-based triple-band rectifier with an impedance matching network is proposed. Figure 15 shows the design diagram of the rectifier. Table 1 shows the geometrical attributes of microstrip lines utilized during the layout of the rectifier. The capacitor C_1 serves as a DC block capacitor, shielding the RF source from unwanted harmonics generated by a diode's nonlinear device [45].

Similarly, the capacitor C_2 is useful for passing only direct current power to the resistive load. [Diode model-SMS7630-079LF (D_1, D_2) from Skyworks and capacitors $C_1 = C_2 = 100$ pF]. In nature, RF signals exhibit sinusoidal behavior, with continuous periodic waves of equal positive and negative amplitudes. The proposed rectifier is built on 1.52-mm-thick Rogers RO4003C substrate. The simulation model needed for the evaluation of the suggested rectifier are managed to perform using the relatively high frequency simulator mostly in advanced design system (ADS). Figure 16 shows the proposed triple-band rectifier's layout configuration setup. The modeling and evaluated outcomes of the rectifier are discussed in the subsequent section.

Results and discussion

After the completion of the necessary simulation studies, the rectifier was manufactured on the PCB machine. The rectifier circuit includes the necessary components of a capacitor, diode, and optimum resistive load for measuring the reflection coefficient and output voltage. The rectifier is now connected to the analyzer (which also provides an RF signal generator) through an SMA connector with an internal impedance of 50 Ω. First, we were using the E8363C PNA network analyzer for measuring the reflection coefficient ($|S_{11}|$) plotted as a function of the suggested rectifying circuit and especially in comparison to the simulated results. Figure 17 demonstrates the computation and evaluated results for the rectifier coefficient of reflection frequency dependence. In the ADS simulator, the S-parameter modeling is used to acquire the triple bands of the proposed rectifier. The first and third bands of the evaluated coefficient of reflection resonance frequency match the simulated results, whereas the second band has a small gap due to impedance mismatch between the input impedance and the rectifier circuit. The proposed rectifier is constructed and simulated for the required frequency bands of 2.7, 3.5, and 4.8 GHz, which seem to be nearer to the antenna resonance frequencies.

The suggested rectifier's frequency response has a magnitude of coefficient of reflection $|S_{11}|$ less than −15 dB. The simulation

https://doi.org/10.1017/S1759078723000880 Published online by Cambridge University Press

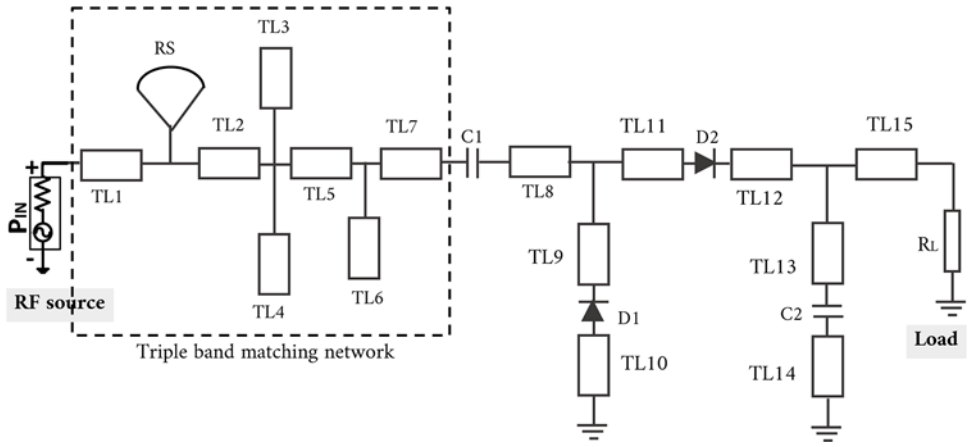

Figure 15. Design diagram of the rectifier circuit.

Table 1. Dimensional values of rectifier circuit

Microstrip line	Length/Width (mm)	Microstrip line	Length/Width (mm)
TL1	11.2/3.6	TL9	9.3/3.6
TL2	12.0/3.6	TL10	10.3/3.6
TL3	19.3/3.6	TL11	5.1/3.6
TL4	15.0/3.6	TL12	9.0/3.6
TL5	9.0/3.6	TL13	12.0/3.6
TL6	10.6/3.6	TL14	10.3/3.6
TL7	6.0/3.6	TL15	12.7/3.6
TL8	4.7/3.6		

model in the ADS simulator is decided to continue to approximate the output voltage at different loading resistance values and input powers utilizing harmonic balance modeling. Modifying the input power from −15 to 20 dBm at specific load resistance values that range from 0.5 to 2.5 kΩ produces output voltages. Figure 18 illustrates the modeling outcomes for rectifier's output voltage. The lower output voltage is obtained at 0.5 kΩ, whereas the higher output voltage is obtained at 2.5 kΩ. The output voltage changes significantly when the input power is changed from −15 to 5 dBm. When the input power exceeds 5 dBm, however, the output voltage becomes saturated. The maximum modeling voltage output of 2.18 V is acquired by concurrently applying all the three frequency responses at the input power of 20 dBm and a resistive load of 2.5 kΩ. Using modeling output voltage values and their corresponding powers and resistive load, the efficiency is determined by calculating equation (1) [15].

$$\text{Efficiency}\ (\%) = \frac{V_0^2/R_L}{P_{in}} \times 100. \tag{1}$$

Figure 19 illustrates the modeling outcomes of the proposed rectifier's determined efficiency versus input power at different loading resistances. At a power input of 0 dBm and a resistive load of 1 kΩ, the suggested rectifier reached a maximum simulation model conversion efficiency of 79.8%. Because of the very small increment of output voltages obtained at these input powers, the conversion efficiency gradually decreases beyond the input power of 0 and 5 dBm. Except for the load impedance of 0.5 kΩ, the suggested rectifier does have an efficiency of more than 30% at relatively low powers of less than 0 dBm for the load resistance values noted in the modeling. As a result, the presented triple-band rectifier is considered suitable for attempting to convert

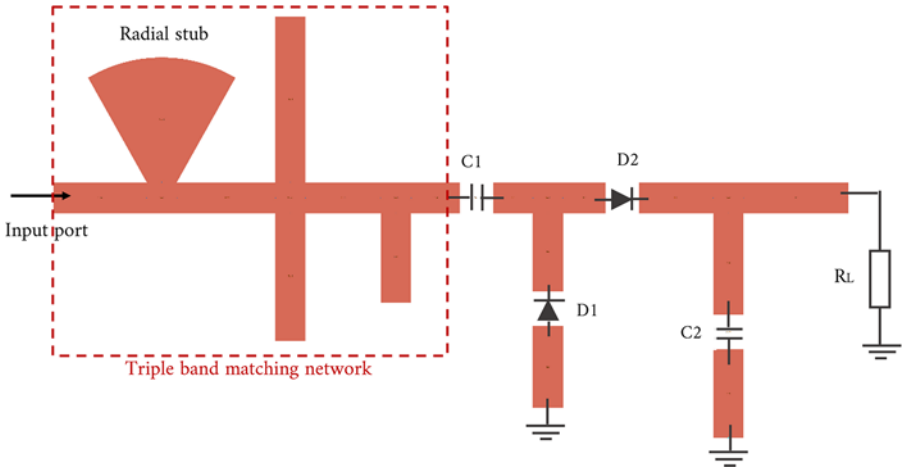

Figure 16. Layout configuration of the rectifier.

https://doi.org/10.1017/S1759078723000880 Published online by Cambridge University Press

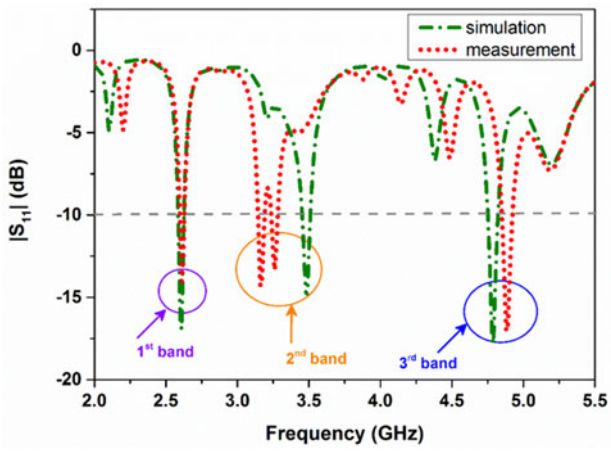

Figure 17. Reflection coefficient ($|S_{11}|$) of the rectifier (input power = 0 dBm, resistive load = 1 kΩ).

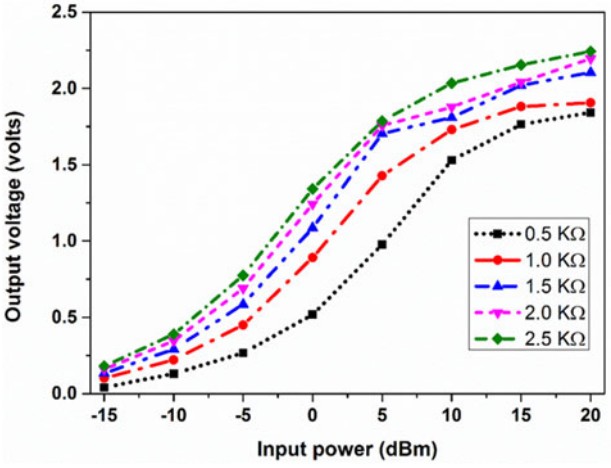

Figure 18. Rectifier's output voltage with input power at various resistive loads.

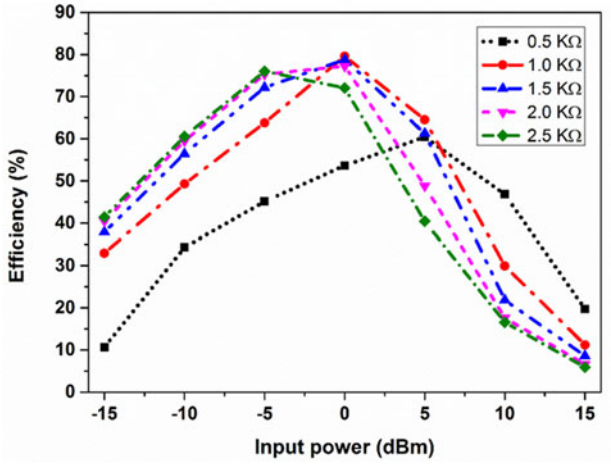

Figure 19. Calculated efficiency with input power at various resistive loads.

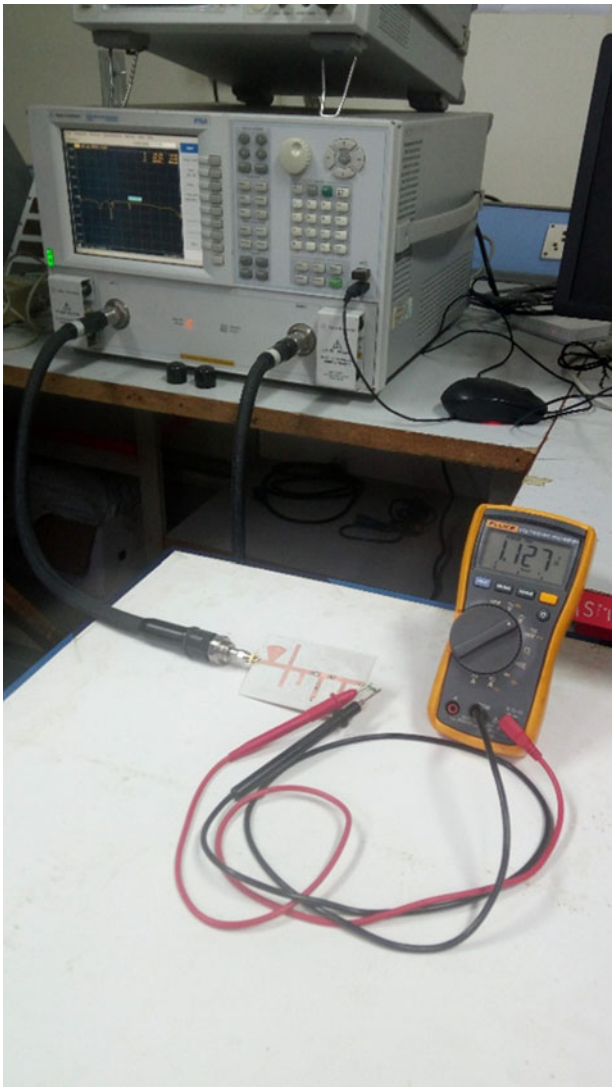

Figure 20. The proposed rectifier's experimental setup for taking measurements of output DC voltage.

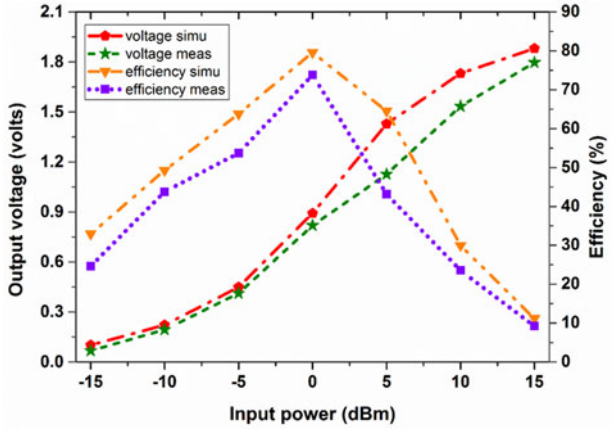

Figure 21. The proposed rectifier's output voltage and efficiency were designed to simulate and evaluated at optimized values.

relatively low RF powers into DC. Following the completion of the simulation studies, the rectifier's output voltage is determined utilizing joint optimization of 1 kΩ load impedance and 0 dBm power supplied. The SMA port of the rectifier is linked to a network analyzer (which serves as an RF power source), and the voltmeter is connected to the load resistance for output voltage measurement.

https://doi.org/10.1017/S1759078723000880 Published online by Cambridge University Press

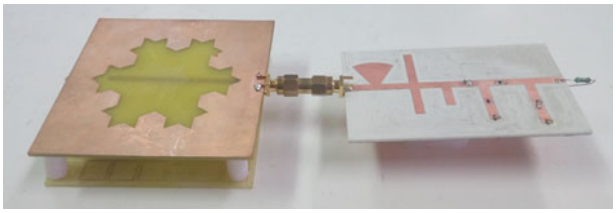

Figure 22. Fabricated prototype of the proposed triple-band rectenna.

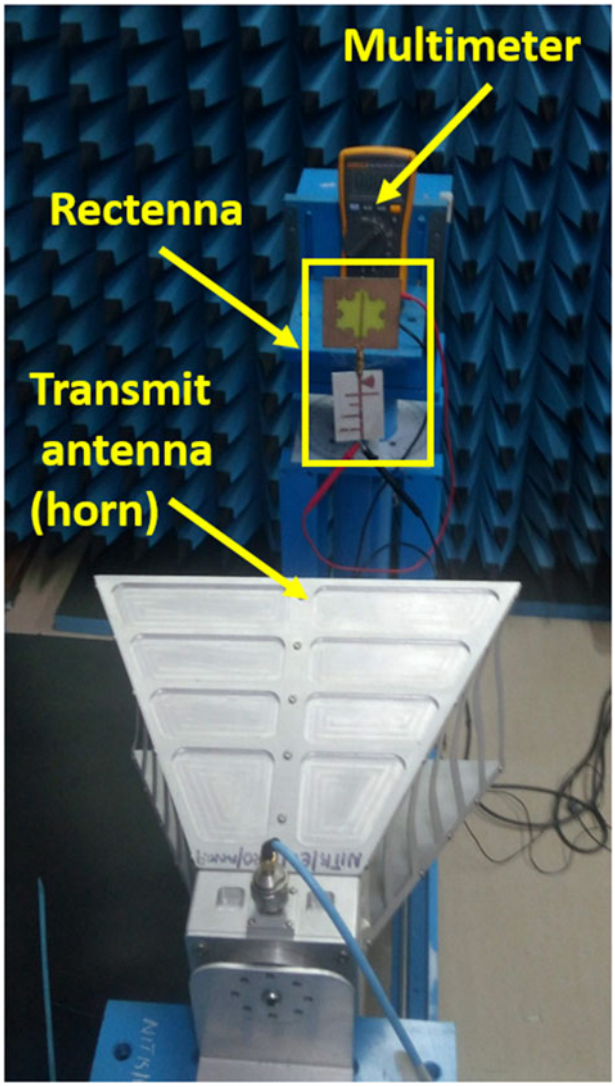

Figure 23. Measurement setup of rectenna in the anechoic chamber.

Figure 20 illustrates an experimental set up for measuring the DC voltage output of the proposed rectifier. The measurement photograph shows that the digital multimeter has a DC voltage output of 1.127 V at the input RF power of 5 dBm. Figure 21 represents the computation and measured output voltage and effectiveness of the rectifier at structure and functionality of 1 kΩ resistive load (R_L) and 0 dBm input power (P_{in}). At the input power of 0 dBm, the peak output voltage and rectifier's efficiency obtained are 1.78 V and 74.3%, respectively.

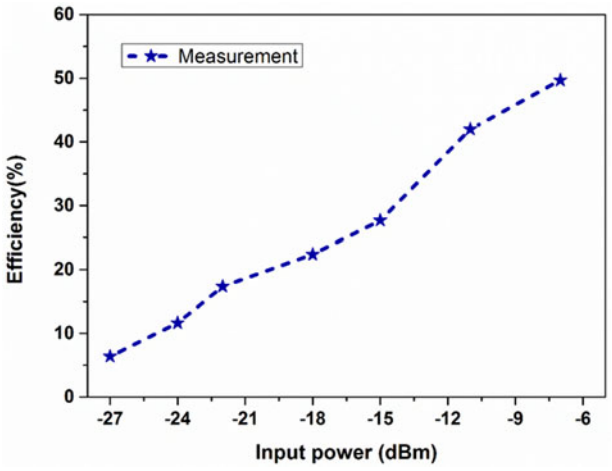

Figure 24. Measured result of conversion efficiency (input power to rectifier).

Rectenna measurement

Figure 22 demonstrates the fabrication prototype of the proposed triple-band rectenna. At the time of evaluating the experiment for output voltage, the rectifier is excited with the received power input from power source connected to the transmit antenna (horn). Figure 23 shows the measurement for rectenna in the anechoic chamber. First, the received power is measured by connecting it to the spectrum analyzer. The transmitting (horn) and receiving (proposed) antennas are positioned at a far-field distance.

The network analyzer's input power is set to 20 dBm maximum value, and the received power is measured using a spike that appears on the display screen. However, the network analyzer input power gradually reduces by 2 dBm and records the received power at each instance. Now, connect the rectifier to the antenna and use the input power mentioned above to measure the output voltage at the load resistor. The efficiency is calculated, and the efficiency with power is analyzed (antenna received power). Figure 24 illustrates the experimental result of efficiency with antenna received power. At optimal values (1 kΩ resistive load and 0 dBm power input), maximum efficiency of 49.67% has been achieved. It is evident from these outcomes that the rectifier integrated antenna is competent of harvesting and trying to convert the necessary high frequency microwave signals into DC. Table 2 shows the proposed triple-band rectenna to certain relevant studies that have already been published. In comparison to [9–12], the proposed rectenna possesses a high conversion efficiency of 74.3%.

Conclusion

A DRS is used to create an equiangular slotted antenna with gain enhanced. To obtain the resonant frequencies without changing the antenna dimensions, a variable FL is used. A Villard voltage doubler is used to implement the transmission line-based triple-band rectifier. High gain antennas with compact sizes other than conventional structures will be more desirable in the future for the development of high-efficient rectennas for Internet of Things, wireless sensor networks, 5G, and low power analog/digital electronic devices. The presented rectifier-integrated antenna is discovered to be appropriate for low level energy harvesting and wireless power transmission.

https://doi.org/10.1017/S1759078723000880 Published online by Cambridge University Press

Table 2. Comparison with some works reported in the publications

Reference	Frequency (GHz)	Antenna dimension (mm^2)	Maximum gain (dB)	Resistive load (kΩ)	Input power (dBm)	Conversion efficiency(%)
[2]	0.915, 2.45	60 × 60	4.18	2.2	−9	37
[3]	1.8, 2.1	190 × 100	13.3	5	−5	48
[5]	0.9, 1.8, 2.1, 2.45	100 × 100	6	11	5.8	84
[7]	0.9, 1.8, 2.1	200 × 175	8.15	5	−10	50
[8]	1.8, 2.1	130 × 80	5.1	1.5	−7	45
[9]	2.5, 3.6	50 × 40	2.6	0.51	2	60
[10]	2.45, 3.5	37 × 35	1.86	1.2	0	60
[11]	2.45	100 × 85	7.6	2	20	75.04
[12]	2–3.1	50 × 35	3.5	4	5	71
This work	2.7, 3.5, 4.8	80 × 80	8.8	1	0	74.3

Competing interests. The author reports no conflict of interest.

References

1. **Shinohara N** (1964) *Wireless Power Transfer via Radiowaves*. Hoboken New Jersey: Wiley.
2. **Niotaki K, Kim S, Jeong S, Collado A, Georgiadis A and Tentzeris MM** (2013) A compact dual-band rectenna using slot-loaded dual band folded dipole antenna. *IEEE Antennas Wireless Propagation Letters* **12**, 1634–1637.
3. **Sun H, Guo YX, Miao H and Zhong Z** (2013) A dual-band rectenna using broadband yagi antenna array for ambient rf power harvesting. *IEEE Antennas Wireless Propagation Letters* **12**, 918–921.
4. **Aboualalaa M, Rahman AB, Allam A, Elsadek H and Pokharel RK** (2017) Design of a dual-band microstrip antenna with enhanced gain for energy harvesting applications. *IEEE Antennas Wireless Propagation Letters* **16**, 1622–1626.
5. **Kuhn V, Lahuec C, Seguin F and Person C**. (2015). A multi-band stacked rf energy harvester with rf-to-dc efficiency up to 84%. *IEEE Transactions on Microwave Theory and Techniques* **63**(5), 1768–1777.
6. **Song C, Huang Yi, Carter P, Zhou J, Yuan S, Qian X and Kod M** (2016) A novel six-band dual cp rectenna using improved impedance matching technique for ambient rf energy harvesting. *IEEE Transactions on Antennas and Propagation* **64**(7), 3160–3171.
7. **Shen S, Chiu CY and Murchg RD** (2017) A dual-port triple-band L-probe microstrip patch rectenna for ambient rf energy harvesting. *IEEE Antennas Wireless Propagation Letters* **16**, 3071–3074.
8. **Khemar A, Kacha A, Takhedmit H and Abib G** (2017) Design and experiments of a dual-band rectenna for ambient RF energy harvesting in urban environments. *IET Microwaves, Antennas & Propagation* **12**(1), 49–55.
9. **Chandrasekaran KT, Agarwal K, Nasimuddin AA, Mittra R and Karim MF** (2020) Compact dual-band metamaterial-based high-efficiency rectenna. *The IEEE Antennas and Propagation Magazine* **62**(3), 18–29.
10. **Wang M, Fan Y, Yang L, Li Y, Feng J and Shi Y** (2019) Compact dual-band rectenna for RF energy harvest based on a tree-like antenna. *IET Microwaves, Antennas & Propagation* **13**(9), 1350–1357.
11. **Ahmed S, Zakaria Z, Husain MN, Ibrahim IM and Alhegazi A** (2017) Efficient feeding geometries for rectenna design at 2.45 GHz. *Electronics Letters* **53**(24), 1585–1587.
12. **Shi Y, Fan Y, Li Y, Yang L and Wang M** (2019) An efficient broadband slotted rectenna for wireless power transfer at LTE band. *IEEE Transactions on Antennas and Propagation* **67**(2), 814–822.
13. **Kamoda H, Kitazawa S, Kukutsu N and Kobayashi K** (2015) Loop antenna over artificial magnetic conductor surface and its application to dual-band rf energy harvesting. *IEEE Transactions on Antennas and Propagation* **63**(10), 4408–4417.
14. **Palazzi V, Hester J, Bito J, Alimenti F, Kalialakis C, Collado A, Mezzanotte P, Georgiadis A, Palazzi L, Roselli L and Tentzeris MM** (2018) A novel ultra-lightweight multiband rectenna on paper for rf energy harvesting in the next generation LTE bands. *IEEE Transactions on Microwave Theory and Techniques* **66**(1), 366–379.
15. **Liu J, Zhang XY and Yang CL** (2018) Analysis and design of dual-band rectifier using novel matching network. *IEEE Transactions on Circuits and Systems II: Express Briefs* **65**(4), 431–435.
16. **Huang M, Lin YL, Ou JH, Zhang XY, Lin QW, Che W and Xue Q** (2019) Single and dual-band rf rectifiers with extended input power range using automatic impedance transforming. *IEEE Transactions on Microwave Theory and Techniques* **67**(5), 1974–1984.
17. **Du ZX and Zhang XY** (2018) High-efficiency single and dual-band rectifiers using a complex impedance compression network for wireless power transfer. *IEEE Transactions on Industrial Electronics* **65**(6), 5012–5022.
18. **Liu Z, Zhong Z and Guo YX** (2015) Enhanced dual-band ambient rf energy harvesting with ultra-wide power range. *IEEE Microwave and Wireless Components Letters* **25**(9), 630–632.
19. **Liu J, Zhang XY and Xue Q** (2019) Dual-band transmission-line resistance compression network and its application to rectifiers. *IEEE Transactions on Circuits and Systems I: Regular Papers* **66**(1), 119–132.
20. **Liu J and Zhang XY** (2018) Compact triple-band rectifier for ambient rf energy harvesting application. *IEEE Access* **6**, 19018–19024.
21. **Song C, Huang Y, Zhou J and Carter P** (2017) Improved ultrawideband rectennas using hybrid resistance compression technique. *IEEE Transactions on Antennas and Propagation* **65**(4), 2057–2062.
22. **Mansour MM and Kanaya H** (2018) Compact and broadband rf rectifier with 1.5 octave bandwidth based on a simple pair of L-section matching network. *IEEE Microwave and Wireless Components Letters* **28**(4), 335–337.
23. **Wu P, Huang SY, Zhou W, Yu W, Liu Z, Chen X and Liu C** (2019) Compact high-efficiency broadband rectifier with multi stage transmission line matching. *IEEE Transactions on Circuits and Systems II: Express Briefs* **66**(8), 1316–1320.
24. **Ou JH, Zheng SY, Andrenko AS, Li Y and Tan HZ** (2018) Novel time-domain schottky diode modeling for microwave rectifier designs. *IEEE Transactions on Circuits and Systems I: Regular Papers* **65**(4), 1234–1244.
25. **Mansour MM and Kanaya H** (2019) High-efficient broadband cpw rf rectifier for wireless energy harvesting. *IEEE Microwave and Wireless Components Letters* **29**(4), 288–290.
26. **Sun H, Zhong Z and Guo YX** (2013) An adaptive reconfigurable rectifier for wireless power transmission. *IEEE Microwave and Wireless Components Letters* **23**(9), 492–494.
27. **Ngo T, Huang AD and Guo YX** (2019) Analysis and design of a reconfigurable rectifier circuit for wireless power transfer. *IEEE Transactions on Industrial Electronics* **66**(9), 7089–7098.

https://doi.org/10.1017/S1759078723000880 Published online by Cambridge University Press

28. **Huang Y, Shinohara N and Mitani T** (2014) A constant efficiency of rectifying circuit in an extremely wide load range. *IEEE Transactions on Microwave Theory and Techniques* **62**(4), 986–993.
29. **Lin YL, Zhang XY, Du ZX and Lin QW** (2018) High efficiency microwave rectifier with extended operating bandwidth. *IEEE Transactions on Circuits and Systems II: Express Briefs* **65**(7), 819–823.
30. **Wu P, Huang SY, Zhou W, Ren ZH, Huang ZLLK and Liu C** (2018) High-efficient rectifier with extended input power range based on self-tuning impedance matching. *IEEE Microwave and Wireless Components Letters* **28**(12), 1116–1118.
31. **Choi J, Xu SJ, Makhoul R and Davila JMR**. (2019). Implementing an impedance compression network to compensate for misalignments in a wireless power transfer system. *IEEE Trans. Power Electron.* **34**(5), 4173–4184.
32. **Xu J and Ricketts DS** (2013) An efficient, watt-level microwave rectifier using an impedance compression network (icn) with applications in outphasing energy recovery systems. *IEEE Microwave and Wireless Components Letters* **23**(10), 542–544.
33. **Lu P, Yang XS and Wang BZ** (2018) Robust rectifying circuits with FET Shunt mounted voltage doubler rectifier. *IEEE Microwave and Wireless Components Letters* **28**(3), 224–226.
34. **Huang Y, Shinohara N and Mitani T** (2017) Impedance matching in wireless power transfer. *IEEE Transactions on Microwave Theory and Techniques* **65**(2), 582–590.
35. **Wang C, Shinohara N and Mitani T** (2017) Study on 5.8-ghz single-stage charge pump rectifier for internal wireless system of satellite. *IEEE Transactions on Microwave Theory and Techniques* **65**(4), 1058–1065.
36. **Zhang Q, Ou JH, Wu Z and Tan HZ** (2018) Novel microwave rectifier optimizing method and its application in rectenna designs. *IEEE Access* **6**, 53557–53565.
37. **Shieh S and Kamarei M** (2018) Transient input impedance modeling of rectifiers for rf energy harvesting applications. *IEEE Transactions on Circuits and Systems II: Express Briefs* **65**(3), 311–315.
38. **Wu P, Huang SY, Zhou W and Liu C** (2018) One octave bandwidth rectifier with a frequency selective diode array. *IEEE Microwave and Wireless Components Letters* **28**(11), 1008–1010.
39. **Pardue CA, Davis AK, Bellaredj MLF, Amir MF, Mukhopadhyay S and Swaminathan M** (2018) Reverse power delivery network for wireless power transfer. *IEEE Microwave and Wireless Components Letters* **28**(7), 624–626.
40. **Zhao F, Li Z, Wen G, Li J, Inserra D and Huang Y** (2019) A compact high-efficiency watt-level microwave rectifier with a novel harmonic termination network. *IEEE Microwave and Wireless Components Letters* **29**(6), 418–420.
41. **Zhang H Guo YX, Zhong Z and Wu W** (2019) Cooperative integration of rf energy harvesting and dedicated WPT for wireless sensor networks. *IEEE Microwave and Wireless Components Letters* **29**(4), 291–293.
42. **Wang X and Mortazawi A** (2019) Rectifier array with adaptive power distribution for wide dynamic range rf-dc conversion. *IEEE Transactions on Microwave Theory and Techniques* **67**(1), 392–401.
43. **Geriki Polaiah KK and M Kulkarni** (2021) Triple-band modified square slotted antenna with enhanced gain for RF energy harvesting *IEEE Madras Section Conference (MASCON)* Chennai, India. pp. 1–8.
44. **Chang TH and Kiang JF**. (2013). Compact multi-band H-shaped slot antenna. *IEEE Transactions on Antennas and Propagation* **61**(8), 4345–4349.
45. SMS7630-079LF Schottky diode Datasheet (2018) Skyworks solutions.

Geriki Polaiah received the B.Sc. and M.Sc. degrees from Sri Venkateswara University, Tirupati, India, in 2005 and 2007, respectively, the M.Tech. degree from the Jawaharlal Nehru Technological University Anantapur, India, in 2010, and the Ph.D. degree from the National Institute of Technology Karnataka, Surathkal, India, in 2022. His research interests include rectifier integrated antennas, rectifying circuits, metasurfaces, and metamaterial-based antennas for microwave wireless power transmission and energy harvesting applications.

https://doi.org/10.1017/S1759078723000880 Published online by Cambridge University Press